**Communications in Advanced Mathematical Sciences**
**Vol. 6, No. 2, 98-103, 2023**
**Research Article**
**e-ISSN: 2651-4001**
**DOI:10.33434/cams.1218552**

# Multistability in a Circulant Dynamical System

Paulo C. Rech*

**Abstract**
In this paper we report on a two parameter four-dimensional dynamical system with cyclic symmetry, namely a circulant dynamical system. This system is a twelve-term polynomial system with four cubic nonlinearities. Reported are some parameter-space diagrams for this system, all of them considering the same range of parameters, but generated from different initial conditions. We show that such diagrams display the occurrence of multistability in this system. Properly generated bifurcation diagrams confirm this finding. Basins of attraction of coexisting attractors in the related phase-space are presented, as well as an example showing phase portraits for periodic and chaotic coexisting attractors.

**Keywords:** Basin of attraction, Circulant dynamical system, Multistability, Parameter-space
**2010 AMS:** 65P20

*Departamento de Física, Universidade do Estado de Santa Catarina, 89219-710 Joinville, Brazil*
***Corresponding author**: paulo.rech@udesc.br
**Received:** 13 December 2022, **Accepted:** 22 May 2023, **Available online:** 30 June 2023
**How to cite this article:** P. C. Rech, Multistability in a Circulant Dynamical System, Commun. Adv. Math. Sci., (6)2 (2023) 98-103.

## 1. Introduction

In this paper we report numerical results referring to a four-dimensional dynamical system with cyclic symmetry, the so-called circulant dynamical system [1], which is modeled by an autonomous nonlinear set of four first-order ordinary differential equations. Such a system was recently proposed by Rajagopal and co-workers [2], being given by

$$\begin{aligned}\dot{x} &= ax + by - y^3,\\ \dot{y} &= ay + bz - z^3,\\ \dot{z} &= az + bw - w^3,\\ \dot{w} &= aw + bx - x^3,\end{aligned} \tag{1.1}$$

where $x$, $y$, $z$, $w$ are the dynamical variables, and $a$, $b$ are the parameters responsible for the type of behavior presented by the system. We draw attention to the fact that the only nonlinearity present in system (1.1) is of the cubic type, and that reports on nonlinear models dominated by such terms are not abundant in the literature. Also, it is important to note that the parameter $a$ must always be negative to guarantee the existence of attractors in the respective phase-space. It is easy to see that negative values of parameter $a$ make system (1.1) dissipative, since is straightforward to show that the flow divergence is equal to $4a$.

System (1.1) was investigated numerically in Ref. [2], both the integer and the fractional order versions. Also, system (1.1) was investigated in Ref. [2] through a circuit design. Bifurcation diagrams with parameter $a$ kept fixed, and parameter $b$ being considered as the bifurcation parameter, were used to detect the presence of the multistability phenomenon. Our contribution to advancing knowledge of this system considers the simultaneous variation of both parameters $a$ and $b$ in the investigation of multistability. In Sect. 2 we report $(a,b)$ parameter-space diagrams which consider the same ranges for the parameters,

but generated from different initial conditions. Such procedure will allow, as we will see in detail in the next section, the detection of multistability areas, instead of the multistability lines obtained in the procedure that uses bifurcation diagrams for this purpose. Finally, concluding remarks are given in Sect. 3.

## 2. The Dynamics in Parameter-Space

Here we report on a numerical experiment related to the investigation of the long-term dynamical behavior of system (1.1). More specifically, five $(a,b)$ parameter-space diagrams are presented, for $-3.5 \leq a \leq -3.0$ and $8.0 \leq b \leq 10.0$. Each of these diagrams was generated in a different way which we will detail in the following, but they all use the largest Lyapunov exponent (LLE), computed by using the algorithm in Wolf and collaborators [3], to characterize the dynamical behavior for each choice of $a$ and $b$ in the respective parameter-space diagram. For each of them the parameter interval was discretized in a grid of $800 \times 800$ points, being system (1.1) numerically integrated by using the fourth-order Runge-Kutta algorithm with a time step equal to $10^{-3}$. The average that must be considered in the computation of each of the $6.4 \times 10^5$ LLEs takes into account $4 \times 10^6$ integration steps, after discarding an appropriate transient. As is well known, system (1.1) has four Lyapunov exponents for each choice of parameters $a$ and $b$, and its dynamical behavior is characterized by the LLE: *(i)* equilibrium point if LLE$< 0$, *(ii)* periodic or quasi-periodic motion if LLE$= 0$, and *(iii)* chaotic or hyperchaotic motion if LLE$> 0$. The main purpose of presenting these five diagrams is to detect differences between the parameter-spaces which, if any, will be a numerical proof of the occurrence of multistability in system (1.1).

Figure 2.1 shows five versions of a same global view of the $(a,b)$ parameter-space of system (1.1), for $-3.5 \leq a \leq -3.0$ and $8.0 \leq b \leq 10.0$. Color in each diagram is related to the magnitude of the LLE. Parameter regions with a positive LLE, painted in a color that ranges from yellow to red, relate to chaotic behavior, while parameter regions in black color stand for periodic solutions and have LLE$= 0$. The small gray region at the bottom left in each diagram, for which the LLE$< 0$, concerns to parameters that lead the system to equilibrium points.

The diagram in Fig. 2.1(a) was generated always from a same arbitrary initial condition, regardless of the values of the parameters $a$ and $b$. Once the set of parameters is defined, system (1.1) is numerically integrated, the respective time series obtained, and the related Lyapunov exponents spectrum is computed. In order to generate the diagram in Fig. 2.1(b) we fix $(a,b) = (-3.5, 8.0)$, and initialize system (1.1) with an arbitrary initial condition. Then system (1.1) is numerically integrated, the respective time series obtained, and the related Lyapunov exponents spectrum is computed. Parameter $a$ is increased, and system (1.1) is initialized with the variables related to the final point obtained for the prior value of $a$. The numerical integration is performed, and a new Lyapunov exponents spectrum is computed from the new time series obtained. Such procedure is repeated until the highest value of $a$, namely $a = -3.0$, is reached. Then parameter $b$ is increased, and the entire procedure is repeated until the parameter set $(a,b) = (-3.0, 10.0)$ is considered in computing. The diagram in Fig. 2.1(c) is constructed in a manner analogous to that in Fig. 2.1(b), but starting from $(a,b) = (-3.0, 8.0)$. Parameter $a$ is decreased until $a = -3.5$. For each increased $b$ until $(a,b) = (-3.5, 10.0)$, this last procedure is repeated. In short, the diagram in Fig. 2.1(b) [Fig. 2.1(c)] was generated by using the method *following the attractor* along lines of constant $b$, increasing (decreasing) $a$ from $-3.5$ ($-3.0$).

Diagrams in Figs. 2.1(d) and 2.1(e) also were generated by using the method *following the attractor*, but in a different way from the one used in the generation of Figs. 2.1(b) and 2.1(c), where each time parameter $b$ is changed the system (1.1) is initialized from a same arbitrary initial condition. This time, however, this initialization happens only once for each of the diagrams. In the case of Fig. 2.1(d), the parameters are fixed at the lowest values $(a,b) = (-3.5, 8.0)$, system (1.1) is initialized from an arbitrary initial condition, and the attractor is followed until the highest values $(a,b) = (-3.0, 10.0)$ are reached. A similar procedure allows generating Fig. 2.1(e), only now going from the highest values $(a,b) = (-3.0, 10.0)$ to the lowest values $(a,b) = (-3.5, 8.0)$.

A cursory glance at the diagrams in Fig. 2.1 misleadingly concludes that they are all identical. However, a closer look reveals that significant differences exist between them. One of these differences appears, for example, in the chaotic stripe in yellow crossed by the small line segment in magenta, which is in the same *geographical position* in each of the diagrams. In two of them, namely in Figs. 2.1(c) and 2.1(e), there is only one periodic stripe in black embedded in this chaotic stripe, while in the other three diagrams there are two periodic stripes in black embedded. Thus, we have just identified a region in the parameter-space of system (1.1), near the magenta line, whose long-term dynamical behavior can be different depending on the initial condition adopted for the numerical integration of system (1.1). In other words, we can say that system (1.1) presents at least more than one coexisting attractors in the phase-space, for a kept fixed set of parameters $(a,b)$ in this region, and this is a signature of the multistability phenomenon [4]. What makes multistable systems worth studying is the fact that this phenomenon has been observed, for a long time, in mathematical models of nonlinear dynamical systems, in the most varied fields of knowledge [5–9].

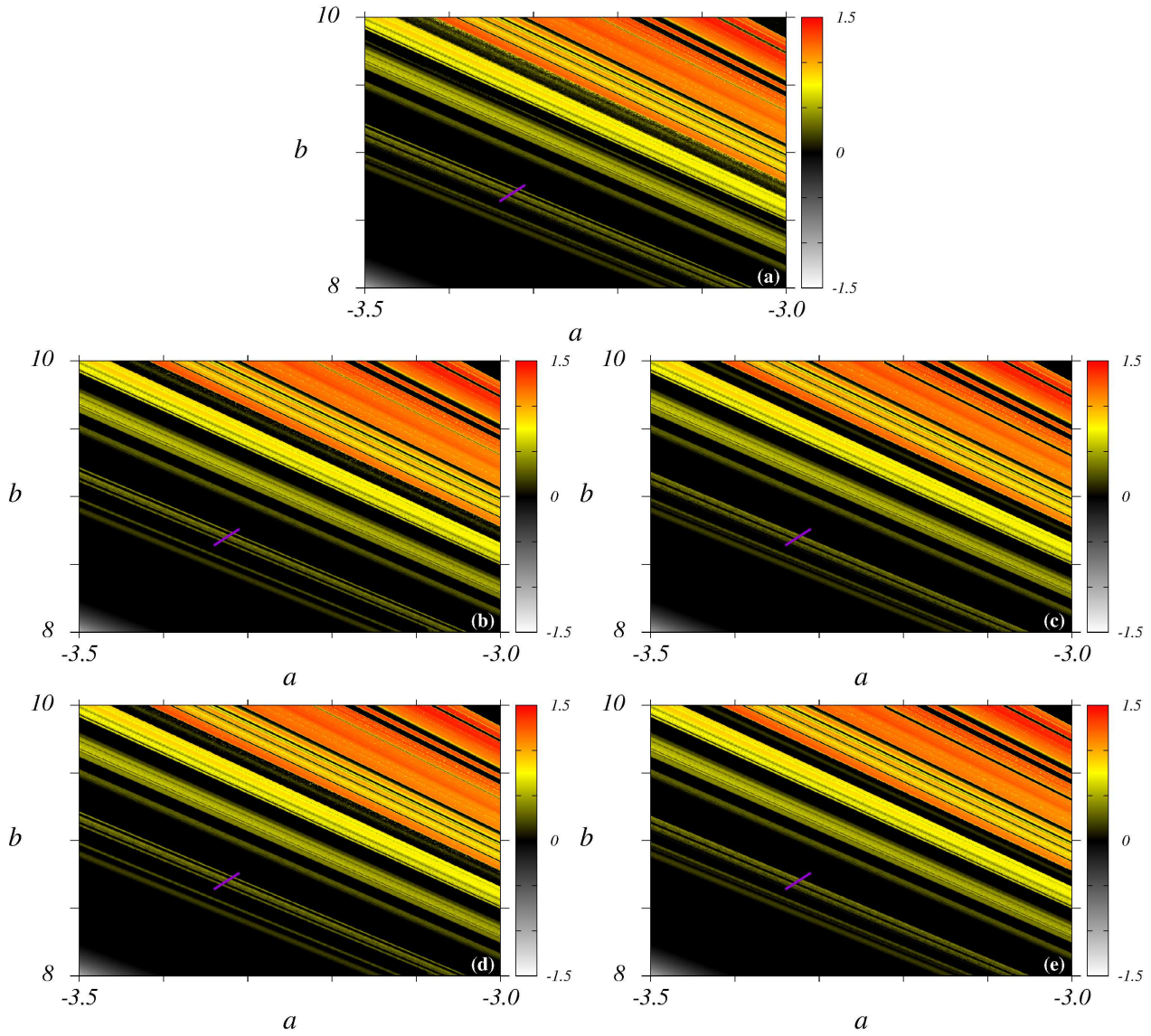


**Figure 2.1.** Regions of different dynamical behaviors in the $(a,b)$ parameter-space of system (1.1). Color in each diagram is related to the magnitude of the largest Lyapunov exponent. (a) Same initial condition, regardless of the values of $a$ and $b$. (b) Following the attractor along lines of constant parameter $b$, from $(a,b) = (-3.5, 8.0)$ to $(a,b) = (-3.0, 10.0)$. (c) Following the attractor along lines of constant parameter $b$, from $(a,b) = (-3.0, 8.0)$ to $(a,b) = (-3.5, 10.0)$. (d) Following the attractor from $(a,b) = (-3.5, 8.0)$ to $(a,b) = (-3.0, 10.0)$. (e) Following the attractor from $(a,b) = (-3.0, 10.0)$ to $(a,b) = (-3.5, 8.0)$.

Figure 2.2 shows two bifurcation diagrams for system (1.1), both generated by *following the attractor*, for points along the line segment $b = 4a + 22$ in magenta connecting the points $(a,b) = (-3.34, 8.64)$ and $(a,b) = (-3.31, 8.76)$ in any of the diagrams in Fig. 2.1. In each of them are shown the local maxima (the peaks) of the variable $x$, commonly called period and denoted by $x_m$, for one thousand values of the parameter $a$. The diagram in blue was generated considering the increase of the parameter $a$ from $-3.34$ to $-3.31$, while that in red considers the decrease of $a$ from $-3.31$ to $-3.34$. There are clear differences between the two bifurcation diagrams in Fig. 2.2 and, as a consequence, a clear evidence of the occurrence of multistability. For example, in the right region, inside the green box for $-3.318 < a < -3.316$, we can observe the coexistence of a chaotic attractor, in red, and a period-5 attractor, in blue.

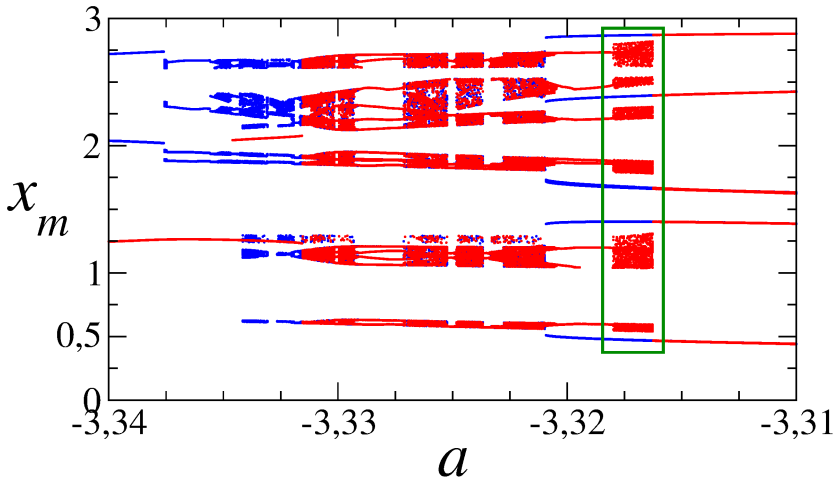


**Figure 2.2.** Two bifurcation diagrams for points along the line segment $b = 4a + 22$ in any of the diagrams in Fig. 2.1. Diagram in blue (red) considers the increase (decrease) of the parameter $a$.

The basins of attraction related to the chaotic and the period-5 attractors, in their respective colors, are shown in Fig. 2.3. In fact, Fig. 2.3 shows a $(x_0, y_0)$ initial condition cross-section of a four-dimensional $(x_0, y_0, z_0, w_0)$ basin of attraction for system (1.1), namely the one for which $z_0 = w_0 = 3.0$, and $(a,b) = (-3.317, 8.732)$, a point belonging to the line segment $b = 4a + 22$ drawn in diagrams of Fig. 2.1. We can see that the basins of the chaotic (in red) and the period-5 (in blue) attractors are not intermingled, that is, the points belonging to one basin are perfectly distinguishable from the points belonging to the other basin. Therefore, the basins of attraction in Fig. 2.3 clearly indicate initial conditions leading to either of the two attractors. Accordingly, since the parameters are kept fixed at $(a,b) = (-3.317, 8.732)$, and for $z_0 = w_0 = 3.0$, any initial condition point $(x_0, y_0)$ chosen in the red region takes the system to a chaotic attractor in the phase-space, whereas any initial condition point $(x_0, y_0)$ chosen in the blue region takes the system to a period-5 attractor.

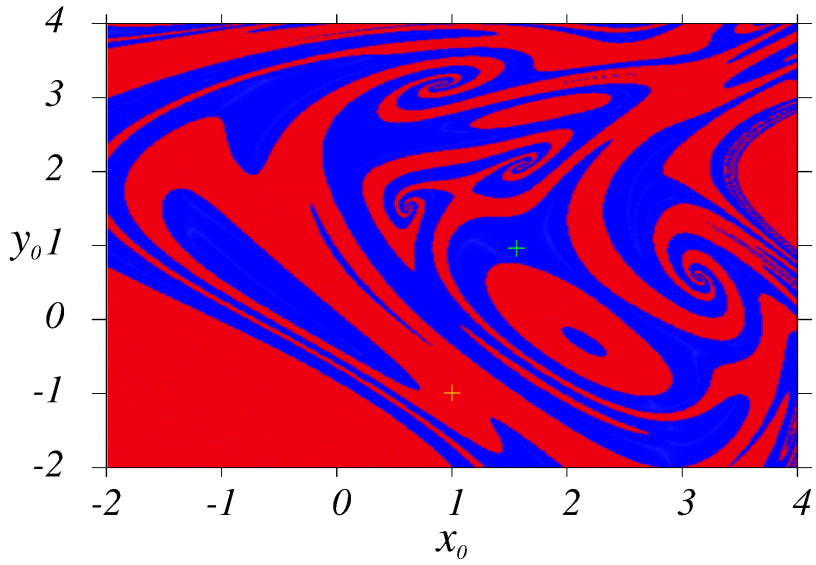


**Figure 2.3.** Projection of basins of attraction for system (1.1) on the $(x_0, y_0)$ initial condition plane, for $z_0 = w_0 = 3.0$. Blue (Red) is related to the period-5 (chaotic) attractor basin.

Figure 2.4 shows two-dimensional projections of the two coexisting attractors, a period-5 and a chaotic, all of them considering the variable $x$ in the horizontal axis, and generated for $(a,b) = (-3.317, 8.732)$. For the period-5 attractor shown in Figs. 2.4(a), 2.4(b), and 2.4(c), the initial condition is $(x_0, y_0, z_0, w_0) = (1.5, 1.0, 3.0, 3.0)$, corresponding to the point marked with a plus sign in the blue region of Fig. 2.3, while for the chaotic attractor shown in Figs. 2.4(e), 2.4(f), and 2.4(g), the initial

condition is $(x_0, y_0, z_0, w_0) = (1.0, -1.0, 3.0, 3.0)$, corresponding to the point also marked with a plus sign, but this time in the red region of the same Fig. 2.3. Figures 2.4(d) and 2.4(h) show the evolution over time of the variable $x$, respectively for the periodic and the chaotic attractors.

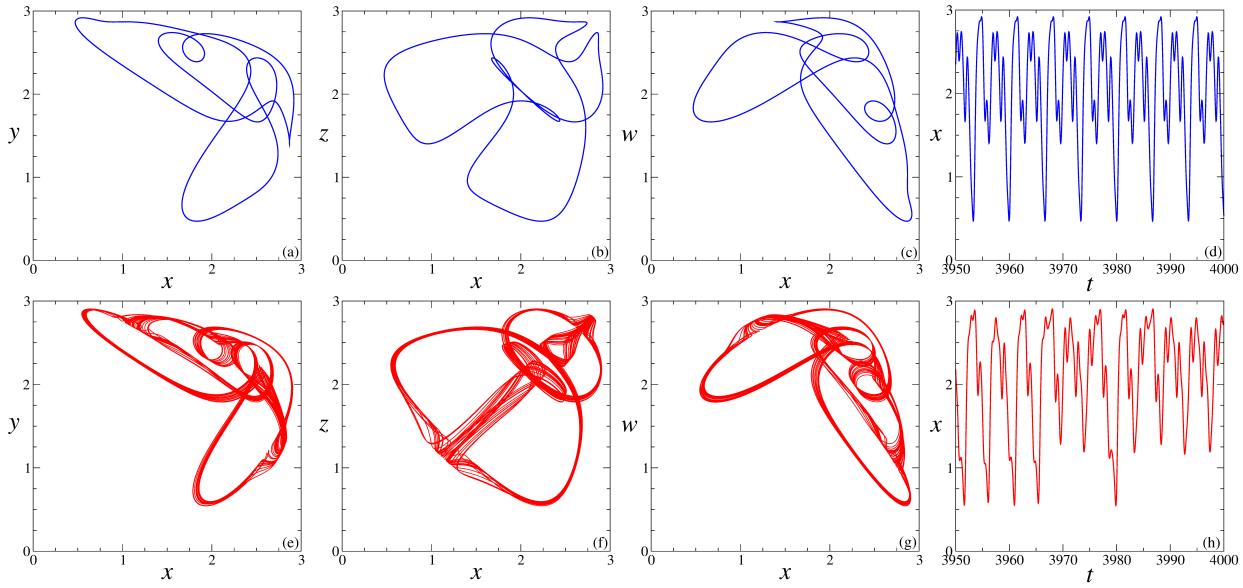


**Figure 2.4.** Two coexisting attractors for system (1.1). In (a) and (b) and (c) are shown projections of the period-5 attractor. In (e) (f) and (g) are shown projections of a chaotic attractor. Diagrams in (d) and (h) show the time series for the variable $x$, respectively for the period-5 and the chaotic attractors.

## 3. Summary and Outlook

We have investigated a two parameter four-dimensional dynamical system, namely a circulant dynamical system modeled by an autonomous set of four first-order ordinary differential equations which presents cubic nonlinearities in all variables, but no crossed nonlinearities. We have reported some versions of a same parameter-space plot of this system, obtained from different initial conditions. Such diagrams present sensitive differences that allow us concluding that multistability is a possible phenomenon in this system for some parameter values. Bifurcation diagrams confirm this finding. As a consequence of the multistability phenomenon, we also have reported on basins of attraction for coexisting periodic and chaotic attractors.

Therefore, we locate and investigate a region in the parameter-space of the circulant dynamical system, in which the model displays coexisting periodic and chaotic attractors, for a same set of parameters. It means the presence of an area in the parameter-space where at least two attractors coexist, depending on the choice of the initial conditions in the numerical integration of the system. As far as I know, such a result has never been reported in the literature of this field of study, for this system. Therefore, this work represents an interesting contribution to advancing knowledge of the system under study, deserving to be read. A possible future work consists of continuing to explore the parameter-space of the circulant dynamical system, in search of other regions that present multistability, including other sets of coexisting attractors, namely periodic-periodic and chaotic-chaotic. We understand, therefore, that the circulant dynamical system deserves further investigation.

With regard to the relevance of the occurrence of multistability in nonlinear dynamical systems, it is important to mention that the phenomenon has been recently reported in several other systems, among them neuron models [10, 11], electronic circuits [12,13], memristor oscillators [14,15], biological systems [16,17], couplings of Duffing and van der Pol Oscillators [18], and snap and jerk systems [19,20], just to name a few among many examples.

## Article Information

**Acknowledgements:** The author would like to express their sincere thanks to the editor and the anonymous reviewers for their helpful comments and suggestions.

**Author's contributions:** The article has a single author. The author has read and approved the final manuscript.

**Conflict of Interest Disclosure:** No potential conflict of interest was declared by the author.

**Supporting/Supporting Organizations:** Grants were received from two public agencies, namely Conselho Nacional de Desenvolvimento Científico e Tecnológico, and Fundação de Amparo à Pesquisa e Inovação do Estado de Santa Catarina.

**Ethical Approval and Participant Consent:** It is declared that during the preparation process of this study, scientific and ethical principles were followed and all the studies benefited from are stated in the bibliography.

**Plagiarism Statement:** This article was scanned by the plagiarism program. No plagiarism was detected.

**Availability of data and materials:** Not applicable.

## References

[1] J. C. Sprott, *Elegant Chaos: Algebraically Simple Chaotic Flows*, World Scientific, Singapore, 2010.

[2] K. Rajagopal, A. Akgül, V. T. Pham, F. E. Alsaadi, F. Nazarimehr, E. Alsaadi, S. Jafari, *Multistability and coexisting attractors in a new circulant chaotic system*, Int. J. Bifurc. Chaos **29** (2019), 1950174.

[3] A. Wolf , J. B. Swift, H. L. Swinney, J. A. Vastano, *Determining Lyapunov exponents from a time series*, Physica D, **16** (1985), 285–317.

[4] U. Feudel, C. Grebogi, *Multistability and the control of complexity*, Chaos **7** (1997), 597–604.

[5] S. M. Hammel, C. K. R. T. Jones, J. V. Moloney, *Global dynamical behavior of the optical field in a ring cavity*, J. Opt. Soc. Am. B **2** (1985), 552–564.

[6] P. Marmillot, M. Kaufman, J. Hervagault, *Multiple steady states and dissipative structures in a circular and linear array of three cells: Numerical and experimental approaches*, J. Chem. Phys. **95** (1991), 1206–1214.

[7] S. J. Schiff, K. Jerger, D. H. Duong, T. Chang, M. L. Spano, W. L. Ditto, *Controlling chaos in the brain*, Nature **370** (1994), 615–620.

[8] F. Prengel, A. Wacker, E. Schöll, *Simple model for multistability and domain formation in semiconductor superlattices*, Phys. Rev. B **50** (1994), 1705–1712.

[9] S. Yoden, *Classification of simple low-order models in geophysical fluid dynamics and climate dynamics*, Nonlinear Anal. Methods Appl. **30** (1997), 4607–4618.

[10] S. Zhang, J. Zheng, X. Wang, Z. Zeng, *A novel no-equilibrium HR neuron model with hidden homogeneous extreme multistability*, Chaos Solitons Fractals **145** (2021), 110761.

[11] C. Gao, S. Qiao, X. An, *Global multistability mechanisms of a memristive autapse-based Filippov Hindmash-Rose neuron model*, Chaos Solitons Fractals **160** (2022), 112281.

[12] L. Zhu, M. Pan, *Hyperchaotic oscillation and multistability in a fourth order smooth Chua system with Implementation using no analog multipliers*, Int. J. Bifurc. Chaos **32** (2022), 2250185.

[13] I. Ahmad, B. Srisuchinwong, M. U. Jamil, *Coexistence of Hidden attractors in the smooth cubic Chua's circuit with two stable equilibria*, Int. J. Bifurc. Chaos **33** (2023), 2330010.

[14] H. Bao, Y. Gu, Q. Xu, X. Zhang, B. Bao, *Parallel bi-memristor hyperchaotic map with extreme multistability*, Chaos Solitons Fractals **160** (2022), 112273.

[15] B. Spagnolo, A. A. Dubkov, A. Carollo, D. Valenti, *Memristors and nonequilibrium stochastic multistable systems*, Chaos Solitons Fractals **164** (2022), 112610.

[16] B. G. Rajni, *Multistability, chaos and mean population density in a discrete-time predator–prey system*, Chaos Solitons Fractals **162** (2022), 112497.

[17] P. P. Singh, B. K. Roy, *Chaos and multistability behaviors in 4D dissipative cancer growth/decay model with unstable line of equilibria*, Chaos Solitons Fractals **161** (2022), 112312.

[18] S. T. Tanekou, J. Ramadoss, J. Kengne, G. D. Kenmoe, K. Rajagopal, *Coexistence of periodic, chaotic and hyperchaotic attractors in a system consisting of a Duffing Oscillator coupled to a Van der Pol Oscillator*, Int. J. Bifurc. Chaos **33** (2023), 2330004.

[19] V. Wiggers, P. C. Rech, *On the dynamics of a Van der Pol-Duffing snap system*, Eur. Phys. J. B **95** (2022), 28.

[20] P. C. Rech, *Self-excited and hidden attractors in a multistable jerk system*, Chaos Solitons Fractals **164** (2022), 112614.